PERSPECTIVE
https://doi.org/10.1038/s41563-020-00858-4

nature materials

Flow and extraction of energy and charge carriers in hybrid plasmonic nanostructures

Suljo Linic ✉, Steven Chavez and Rachel Elias

Strong interactions of electromagnetic fields with plasmonic nanomaterials have been exploited in various applications. These applications have centred on plasmon-enhanced scattering rates in nearby molecules or plasmon-induced heating. A question that has emerged recently is whether it is possible to use plasmonic nanostructures in a range of hot electron (hole) applications, including photocatalysis, photovoltaics and photodetection. These applications require coupling of a plasmonic component, which amplifies the interaction of light with the material, to an attached non-plasmonic component that extracts this energy in the form of electronic excitations to perform a function. In this Perspective, we discuss recent work in the emerging field of hybrid plasmonics. We focus on fundamental questions related to the nanoscopic flow of energy and excited charge carriers in these multicomponent materials. We also address critical misconceptions, challenges and opportunities that require more attention.

Plasmonic nanostructures, such as nanoparticles of Au, Ag, Cu and Al, have emerged as an important class of optically active materials. The initial interest in these materials was based on their high ultraviolet–visible optical cross-sections, manifested in enhanced oscillating electric fields concentrated in small volumes around the surface of and within the nanostructures[1–4]. This property of plasmonic nanoparticles to concentrate the light energy at their surface has been exploited in many applications, including surface (plasmon)-enhanced Raman spectroscopies (SERS)[5–7], enhancement of second harmonic generation[8,9], and enhanced sensing of fluorescently labelled entities in biological systems[10,11]. In these applications, the plasmon-induced electric field leads to increased rates of optical scattering from a molecule that is placed within this field[1].

A question that has emerged recently is whether it is possible to take advantage of the physical properties of plasmonic nanostructures for additional applications that go beyond just increasing scattering rates in nearby molecules. For example, one can envision a multicomponent hybrid material, where a plasmonic component amplifies and concentrates the light energy within the material, and an attached non-plasmonic component extracts this energy in the form of electronic excitations (energetic electron–hole (e–h) pairs) to perform a function[12]. Examples of these hybrid materials include plasmonic-metal/metal, plasmonic-metal/semiconductor and plasmonic-metal/molecule systems[3,4,13–16]. At the core of these applications is a flow of energy across plasmonic/non-plasmonic interfaces.

In this Perspective, we discuss the emerging field of hybrid plasmonic materials ('hybrid plasmonics'). The central question we explore is how the optical, physical and chemical properties of a plasmonic nanoparticle change when a small amount of another material (that is, molecules or thin layers/small clusters of different metals or semiconductors) is attached to its surface to form a hybrid plasmonic material. Our aim is to shed light on the potential of these hybrid nanostructures to control the flow of energy across plasmonic/non-plasmonic interfaces, therefore opening up avenues for engineering new families of energy conversion devices (photovoltaics, photocatalysts, photodetectors and so on). We also discuss common misconceptions and fundamental questions that deserve more attention, as well as related challenges and opportunities. We complete the Perspective by describing a few recent examples of the practical applications of hybrid plasmonic materials.

Plasmon excitation and decay in metal nanoparticles

We begin by discussing the processes taking place when a clean plasmonic nanoparticle interacts with electromagnetic radiation. This interaction leads to enhancements in the optical extinction cross-section accompanied by an increase in the oscillating surface electric fields at the resonant frequencies (Fig. 1a). At these frequencies, conduction electrons coherently couple with the photon electric field, creating localized surface plasmon resonance (LSPR) excited states. From a macroscopic perspective, the particle is coherently polarized. From a quantum perspective, the LSPR excited state has been described as a coherent superposition of low-energy electrons and holes near the Fermi level (E_F)[17,18]. This collective electronic oscillation state decays within a few femtoseconds (~10 fs) via photon scattering into the far field or by creating (in most cases) single e–h pair excitations within the nanoparticle, with the energy of these e–h pairs equal to the photon energy (Fig. 1b(i))[19]. For clean plasmonic nanoparticles, the process of photon scattering, whose rate constant is proportional to the square of the particle volume, dominates plasmon relaxation for relatively large particles of Ag and Au (over ~70 nm), while for smaller nanoparticles (less than ~20 nm) the e–h pair formation (that is, photon absorption) is the dominant process[20,21].

The e–h pair formation in the nanoparticle can proceed via the following mechanisms[22]: (1) indirect phonon-assisted intraband (*s*-to-*s*) transitions from the *s* states below E_F to the *s* states above E_F. In this process, another body (for example, a phonon) is required to conserve the electron momentum. The rate constant (the inverse of the plasmon relaxation time) for this excitation mechanism is $\gamma_{ph} \approx 10^{13}$–$10^{14}$ s^{-1} for nanoparticles that are tens of nanometres in diameter[22,23]. (2) Momentum conserved (that is, allowed) formation of multiple e–h pairs from a single photon. The rate constant for this process is $\gamma \approx 10^{15}(E_{ph}/E_F)^2$ s^{-1}, where E_{ph} is the photon energy. For visible photons impinging on Ag, the probability for this process

University of Michigan, Ann Arbor, MI, USA. ✉e-mail: linic@umich.edu

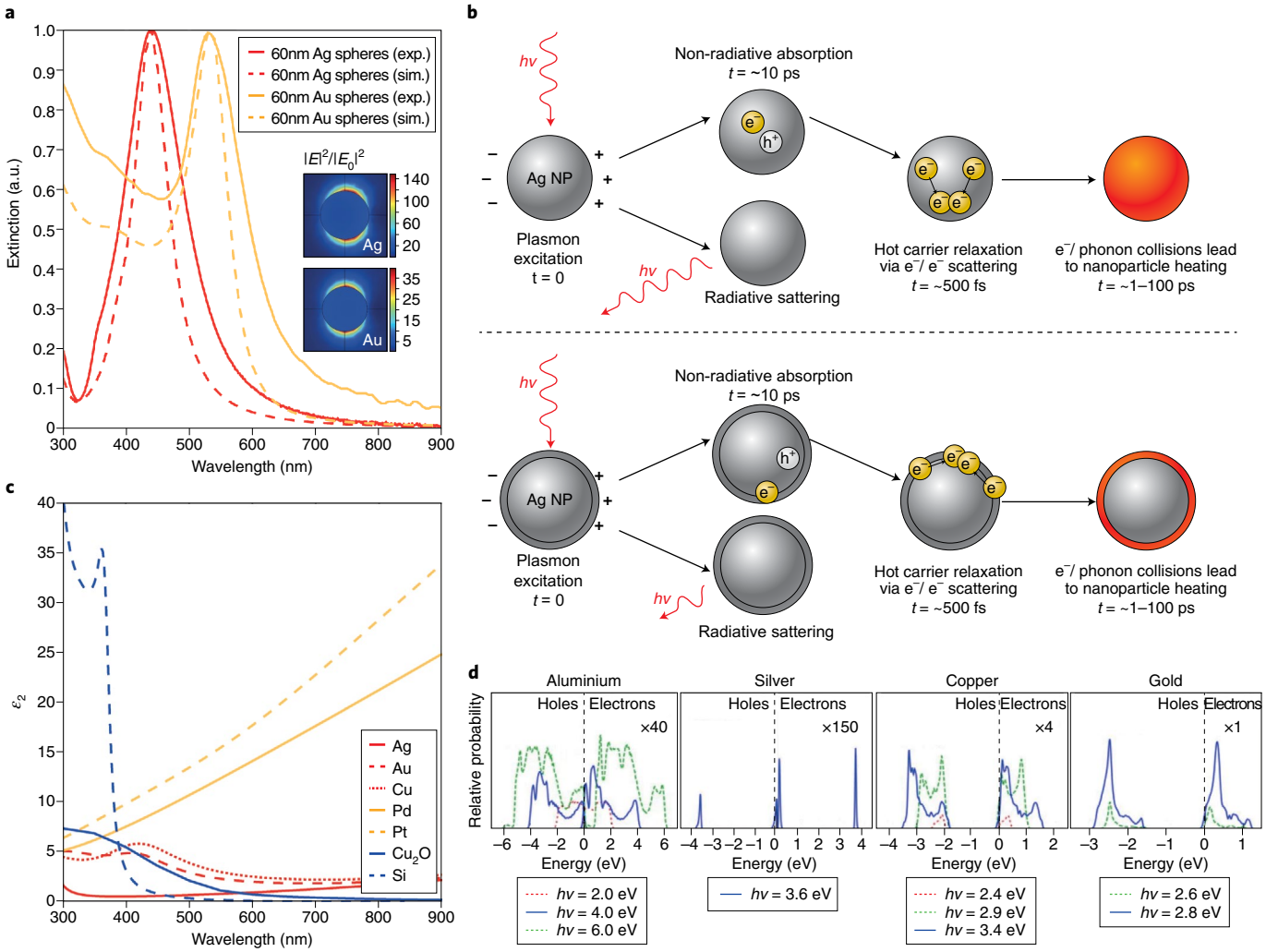

Fig. 1 | Characteristics of plasmon excitation and decay. a, Normalized experimental and simulated extinction spectra for 60 nm Ag spheres and 40 nm Au spheres in water illustrate large optical cross sections at LSPR wavelengths. Corresponding contour plots for the simulated electric field enhancement, $|E|^2/|E_0|^2$, at the respective LSPR wavelengths for these particles in water (inset). **b**, Illustration of sequential plasmon excitation and decay processes in: (1) an illuminated monometallic Ag nanoparticle and (2) Ag nanoparticle with another material attached to the nanoparticle surface. Note that in the hybrid material, a larger fraction of carriers is initially generated either directly in the non-plasmonic shell or at the interface between the nanoparticle and the attached material. **c**, The imaginary part of the dielectric function for various plasmonic and non-plasmonic materials. **d**, The initial energetic charge carrier energy distributions at various photon energies (solely due to *d*-to-*s* transitions) for aluminium, silver, copper and gold. Hot electrons (holes) are indicated via positive (negative) energies relative to the Fermi level. While Cu and Au are dominated by characteristic high energy holes, Al exhibits a more uniform energy distribution and Ag exhibits a bimodal energy distribution of electrons and holes. Panel **d** adapted with permission from ref. [33], Springer Nature Ltd.

is ~10^{13}–10^{14} s^{-1}, and this process becomes more relevant at higher photon energies[24]. (3) Indirect geometry-assisted intraband *s*-to-*s* transitions. Here, the momentum is conserved by an electron collision with the surface in the so-called Kreibig decay[25–28]. The rate constant for this excitation is dependent on the size of the particle, and it can be described using $\gamma_{geo} \approx v_F/R$, where v_F is the Fermi velocity and R is the radius of the nanoparticle. For Ag nanoparticles, the rate constant for these transitions is ~10^{14} s^{-1} for nanoparticles with a diameter of ~10 nm and ~10^{13} s^{-1} for nanoparticles with a diameter of ~100 nm (ref. [22]). (4) Direct momentum conserved photon absorption by electron excitation from the *d* states below E_F vertically up to the *s* states above E_F, often referred to as interband (*d*-to-*s*) transitions. While rate constants for these transitions are wavelength-dependent, when they are energetically accessible the transition rates are higher compared to the above described phonon-mediated *s*-to-*s* excitations[22,29,30]. The accessibility of these transitions at the given wavelength for different metals depends on the location of the metal *d* states relative to E_F. For instance, Ag *d*-to-*s* interband excitations cannot be induced by visible light photons, since the *d* band of Ag lies well below E_F. Au and Cu are also characterized by a full *d* band; however, the energies of these *d* bands are higher compared to Ag, so visible light photons above a specific threshold energy can induce *d*-to-*s* interband excitations in these metals. In contrast to noble metals, the *d* states for the non-noble transition metals (Pt, Pd and so on) are not completely full, and they intersect E_F. As a result, these metals can absorb photons via interband excitations throughout the visible range.

The macroscopic parameter that describes these different photon absorption processes is the imaginary part of the dielectric function, ε_2, which is shown in Fig. 1c for various materials. This parameter describes the bulk materials and does not account for the particle geometry-specific Kreibig surface decay mechanism.

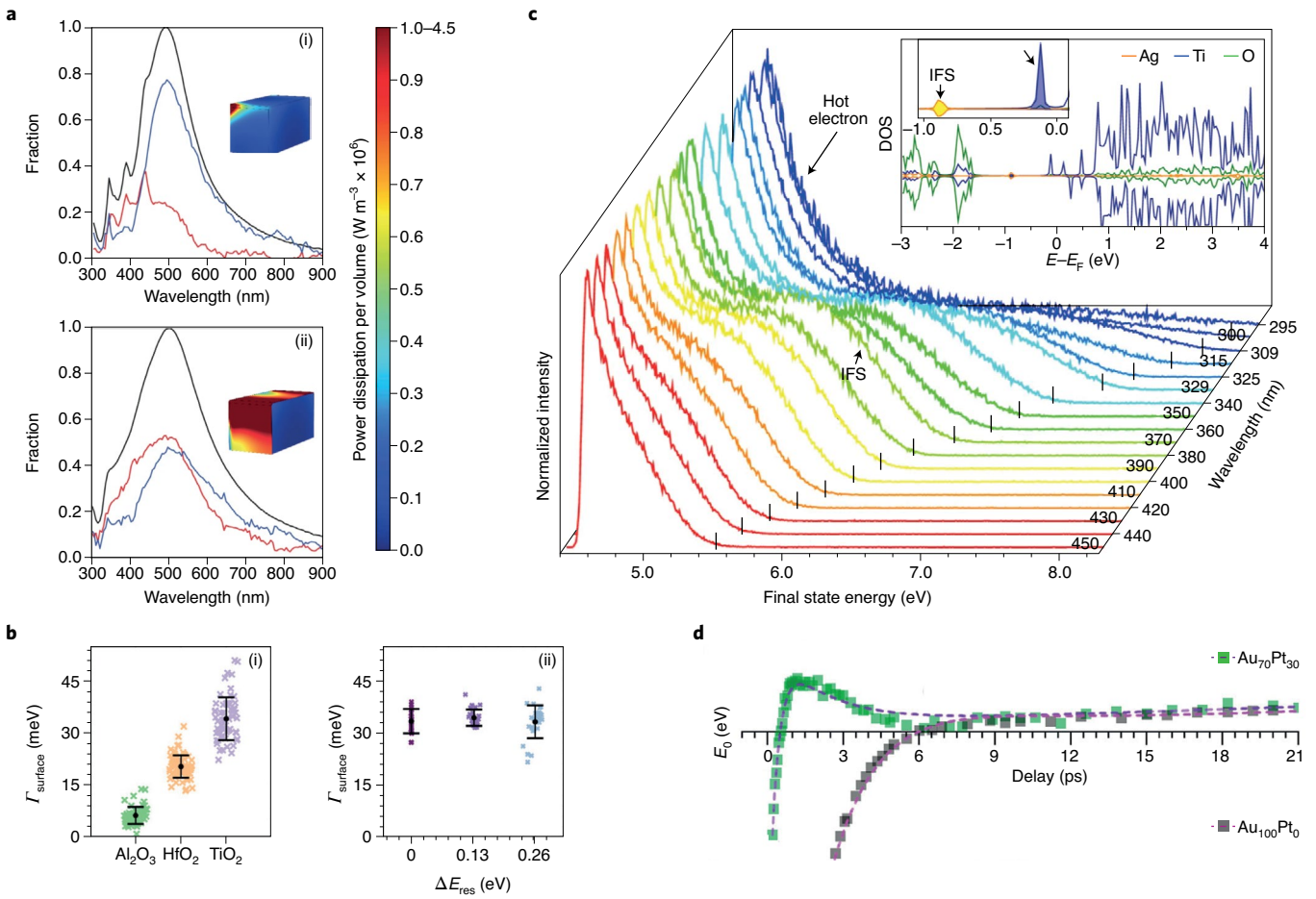

Fig. 2 | Plasmon decay in hybrid plasmonic nanostructures. a, Experimental extinction, absorption, and scattering fractions for: (i) Ag nanocubes (75 nm edge length) and (ii) Ag–Pt core-shell nanocubes (75 nm Ag plus 1 nm Pt). The addition of Pt substantially enhances the fraction of light absorbed by the nanostructures. The corresponding contour plot insets show the simulated power dissipation per volume within one corner quadrant of the nanoparticles at the LSPR frequencies at identical illumination power. The plots indicate that the absorption in the Ag–Pt structure takes place predominantly in the Pt shell. **b**, Ultrafast two-photon photoemission spectra of Ag clusters on TiO_2 shows evidence of the critical importance of the interfacial Ag–TiO_2 state (IFS) in the decay of Ag LSPR. Inset provides the first principles calculated density of states (DOS) for an Ag_3/TiO_2 system, confirming the assignment of the IFS. The top left of inset shows the enlarged DOS around the bandgap of TiO_2 highlighting the IFS at −0.9eV in yellow. The IFS is characterized by a chemical bond formed between Ag and O atoms at the interface. Experiments were performed with a pulse frequency of 1.25 MHz with average excitation powers between 0.1 and 20 mW. **c**, Average contribution ($\Gamma_{surface}$) to the total LSPR decay rate due to different Au/oxide interfaces: (1) $\Gamma_{surface}$ for Au/oxide (oxide = Al_2O_3, HfO_2, TiO_2) interfaces. The data indicates that plasmon decay rate is sensitive to the presence of different materials at the interface; (2) $\Gamma_{surface}$ plotted as a function of Au nanorod plasmon resonance shift (ΔE_{res}) for several Au/TiO_2 systems of varying TiO_2 layer thicknesses suggests that $\Gamma_{surface}$ is independent of layer thickness. **d**, Transient absorption spectroscopy measured LSPR peak energy (E_0) as a function of time for Au nanocrystals (black) and Au@Pt nanocrystals (green) illustrates the shift in delay time from 2 ps (for Au) to 0.6 ps (in AuPt), indicating faster energy transfer (larger LSPR decay rates) in the case of AuPt. Experiments performed using 512 nm pump pulses (80 fs, 350 μJ pulse^{-1} cm^{-2}) on the sample. Figure adapted with permission from ref. [12], Springer Nature Ltd (**a**); ref. [38], Springer Nature Ltd (**b**); ref. [39], American Chemical Society (**c**); and ref. [40], American Chemical Society (**d**).

As explained above, due to the inaccessibility of *d*-to-*s* transitions, it is not surprising that ε_2 is smallest for Ag across a wide wavelength range, while it is larger for Au and Cu, and even larger for other materials.

An inspection of the decay rates (1 to 4 above) indicates that all the proposed mechanisms can play a role in the plasmon decay. The exact magnitude of each mechanism and therefore the energy of generated charge carriers, as well as the location of their initial generation and transport properties, depend on the geometry (size and shape) and elemental nature of the plasmonic nanoparticle. For example, due to the inherently larger rate constant of the momentum-conserved, 'allowed' *d*-to-*s* excitations compared to the *s*-to-*s* excitations, plasmon decay via these excitations is critically important when these states are energetically accessible (for example, in Au and Cu)[31]. Additionally, plasmon decay via the surface-mediated Kreibig excitations (which is critical for small nanostructures) pushes the initial e–h formation to the surface as demonstrated in several recent experimental and theoretical studies[27,32]. We also note that due to the symmetric nature of the *s* band around the Fermi level in metals, an initial decay of a plasmon through the *s*-to-*s* transitions has a high probability of generating equally energetic electrons and holes in the *s* band. On the other hand, the excitation of interband *d*-to-*s* transitions generates an asymmetric distribution of low-energy *s* electrons and high-energy *d* holes (Fig. 1d)[33]. These *d* holes have low mobility and are therefore difficult to extract. This high degree of complexity stipulates

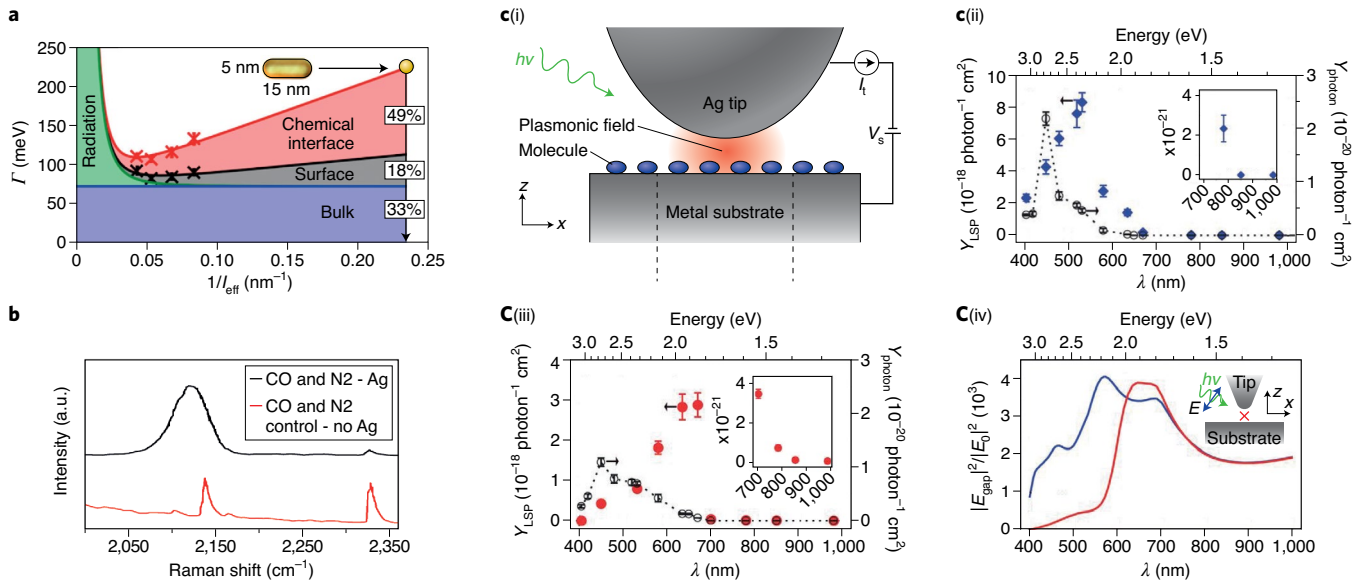

Fig. 3 | Demonstrations of energy and charge transfer in hybrid plasmonic systems. a, Experimentally measured plasmon line width (Γ), proportional to the LSPR decay rate, as a function of the inverse electron mean free path, l_{eff} (where $1/l_{eff}$ is a proxy for nanoparticle size) for different sized Au nanorods. Nanorods are encapsulated in ethanol (black crosses) or DDT (red crosses). Relative contributions from the four plasmon decay mechanisms are highlighted in the shaded regions, showing that chemisorption-induced interfacial states play an increasing role with decreasing particle size. The increase in Γ on DDT-encapsulated nanorods compared to ethanol suggests that interfacial states induced by molecular chemisorption become significant for plasmon decay. **b**, SERS spectra for equimolar CO (left peaks) and N_2 (right peaks) adsorbed on Ag (black) and a control experiment with no silver (red) indicate that the SERS enhancement for CO is significantly larger than for N_2, despite similar Raman cross sections. **c**, Demonstrations of a plasmon-mediated molecular dissociation reaction on a metal surface. (i) Schematic of a scanning tunnelling microscopy (STM) setup consisting of an Ag tip in nanoscale proximity to dimethyl disulfide molecules bound to a metal substrate. Dependence of the surface plasmon-induced dissociation yield (Y_{LSP}) for dimethyl disulfide on the Ag(111) surface (ii) and Cu(111) surface (iii), with metal substrates held at 5 K under ultrahigh vacuum. Black circles represent photodissociation yields without plasmon excitation (Y_{photon}). (iv) Calculated electric field enhancement in the gap between the STM tip and the Ag (blue) and Cu (red) surfaces. Figure adapted with permission from ref. [42], American Chemical Society (**a**); ref. [47], Springer (**b**); and ref. [69], AAAS (**c**).

that any quantitative modelling of plasmon decay processes, even in monometallic nanostructures, requires a complete metal- and geometry-specific electronic structure of the material that goes well beyond simple approximations such as the jellium model[34].

Plasmon decay via photon absorption in hybrid materials

Let us now examine how the plasmon decay process changes when a small amount of another non-plasmonic material (molecules, thin layers or small clusters of different metals or semiconductors) is attached to the surface of a plasmonic nanoparticle to form a hybrid plasmonic material. We note that even if this layer of non-plasmonic material covers the entire nanoparticle, as long as it is relatively thin (for most materials up to 1 nm), incoming light will reach the plasmonic component and induce a plasmonic excitation. From the electronic structure perspective, this non-plasmonic entity often supports direct momentum-conserved electronic excitations (akin to the *d*-to-*s* transitions, mechanism 4 above) at LSPR frequencies. Also, due to the formation of the chemical bonds between this entity and the plasmonic metal, local interfacial electronic states arise that are shared between the two materials. In most cases, these interfacial states also allow for the direct momentum conserved excitations[30].

Based on this reasoning, we postulated that the formation of hybrid plasmonic materials in most cases means that additional, location-specific pathways become available for the initial e–h pair formation to take place (for example, at the plasmonic/non-plasmonic interface or directly within the non-plasmonic material). This influences the location of the initial energetic e–h pair formation within the hybrid nanostructure (Fig. 1b(ii)) and has critical consequences on the flow and dissipation of energy within the hybrid material. To test these hypotheses, we studied the processes of photon absorption in several hybrid plasmonic systems. In one of these studies, we analysed the changes in photon absorption induced when we deposited a ~1.0–1.2-nm-thin shell of Pt onto a plasmonic Ag nanocube core with a ~75 nm edge length (Fig. 2a)[12]. The measurements showed that the hybrid Ag–Pt material exhibits optical extinction due to the excitation of LSPR, similar to monometallic Ag nanoparticles. In monometallic Ag nanocubes, most of the electromagnetic energy was scattered into far field, consistent with high scattering rates of these relatively large Ag nanoparticles (Fig. 2a(i)). On the other hand, a substantially larger fraction of energy was absorbed in the Ag–Pt core-shell nanostructures (Fig. 2a(ii)). Furthermore, we found that in Ag–Pt, the process of the initial energetic e–h pair formation was almost exclusively confined to the Pt shell, that is, to the surface regions of the hybrid material (insets of Fig. 2a).

An analysis of the underlying mechanisms uncovered two factors that play crucial roles in the preferential energy dissipation through the Pt shell[35]. One factor is that, for visible photon energies, ϵ_2 is larger for Pt compared to Ag (Fig. 1c). Therefore, there is a natural preference for energy to be dissipated through the absorption in the Pt shell. Another factor is that this Pt absorption channel is further enhanced by the presence of high LSPR-induced oscillating electric field intensities at the surface layers of these nanostructures (where the Pt layers reside). We note that the rate of optical excitation is proportional to the intensity of the local electric field (E^2)[36]. We demonstrated that the same physical mechanism was in action when thin layers of molecular dyes or a semiconductor were deposited on Ag nanoparticles[37].

The proposed mechanistic hypotheses have recently been tested in a number of transient absorption pump–probe measurements,

ultrafast two-photon photoemission (2PP) spectroscopy measurements, and LSPR lifetime measurements on a single nanoparticle level[38–41]. In one of these studies, 2PP spectroscopy was used to measure the LSPR decay with high spatial and temporal resolution in a hybrid system containing Ag nanoparticles deposited on TiO_2 (ref. [38]). It was demonstrated that the LSPR decay generated non-thermal electrons on a <10 fs timescale. These hot electrons almost exclusively originated from the interfacial electronic states, formed in the process of the chemical attachment of Ag to TiO_2 (Fig. 2b). The results supported the notion that the interfacial Ag–TiO_2 states opened up fast energy dissipation channels (mechanism 4 above), and that the location of the initial energetic e–h formation (due to LSPR decay) proceeded through these interfacial states. Similar observations were made in the direct measurements of the plasmon decay rates at a single particle level for Au nanoparticles coated with different metal oxides[39]. The measurements showed that the LSPR decay rate was governed by the availability of energetically accessible electronic states at the interface of Au and metal oxides (Fig. 2c), indicating that the decay proceeded through these interfacial states. In yet another study, transient absorption spectroscopy was employed to investigate the ultrafast photodynamics of small (~8 nm) Au–Pt core-shell nanospheres[40]. It was demonstrated that up to 80% of the photon energy was deposited in the ultrathin Pt shell on extremely short lifetimes in the case of Au–Pt (Fig. 2d).

These recent mechanistic findings, derived in pulsed as well as in continuous-wave illuminations studies, paint a consistent picture of photon absorption in hybrid plasmonic materials and also shed light on several previously made observations. For example, it has been known that the LSPR decay rate can be changed (often enhanced) when molecules (or other entities) are chemisorbed on the surface of plasmonic nanoparticles. This observation, loosely labelled 'chemical interface damping of plasmons', was initially reported by Träger et al. in their spectral hole burning measurements and was more recently supported by a number of single particle measurements[30,32,42–46]. These measurements showed the rate of LSPR decay was heavily influenced by the nature of an absorbed molecule, suggesting that the interfacial molecule/particle states played a critical role (Fig. 3a)[42]. Furthermore, the literature is full of examples where plasmonic enhancements in Raman spectroscopy are much larger than those predicted by the plasmon electric field enhanced Raman scattering rates[5,47–49]. For instance, CO molecules have a much larger LSPR-induced enhancement in the SERS signal compared to N_2 molecules on an identical plasmonic material—despite similar free-molecule Raman cross-sections (Fig. 3b)[47]. These discrepancies are usually explained by invoking a 'chemical enhancement' mechanism, wherein electronic charge is somehow exchanged between the nanoparticle and molecule, giving rise to additional enhancements in the Raman scattering rates akin to the resonant Raman excitation process. We believe that the interface-mediated LSPR decay mechanism, explained in the previous paragraphs, can explain both the chemical enhancements in SERS and chemical interface damping processes. This mechanism suggests that these processes should be important when there are local electronic states at the nanoparticle/molecule interface that can be excited by the high local surface plasmonic fields.

Common misconceptions and moving the field forward

It is critical to discuss some common misconceptions related to extracting charge/energy in hybrid plasmonic systems. Two important sources of these misconceptions are the assumptions that: (1) energetic charge carriers are initially formed at a homogeneous rate throughout the material, and (2) since their lifetime is short as they thermally equilibrate with nanoparticle phonon modes on the order of ~10 ps, the charge carriers cannot be involved in surface (interface) processes. A common corollary to this is an often-discussed claim that the light-induced, macroscopic and

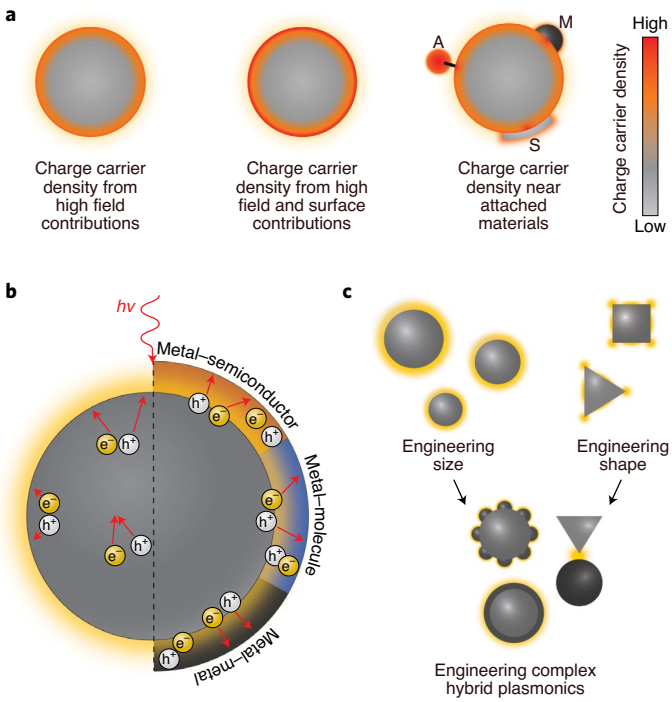

Fig. 4 | Engineering energy flow in hybrid plasmonic systems. **a**, Illustration of the factors that impact the location specific initial rates of charge carrier formation due to LSPR decay. The rates are impacted by high surface fields (left), the rate at which the plasmon collides with the surface—which is higher for small particles (middle), and the presence of non-plasmonic materials at the surface (or interfacial states at the plasmonic/non-plasmonic interface) that allow for the direct electronic excitations (right). Non-plasmonic materials could be a molecule (A), a metal nanoparticle (M), and/or a semiconductor (S). **b**, Electron–hole pair generation and transport in a clean plasmonic nanostructure (left) and in one coated with either a semiconductor, molecules or another metal. The charge carriers are generated throughout the entire volume of the clean plasmonic nanoparticle, while the process is confined to either the attached material or the interface between the attached material and the nanoparticle in the hybrid system. **c**, Schematic of various geometries and configurations of hybrid plasmonic nanostructures. Material science advances in the synthesis of uniform and stable nanostructures, with precise control over size, shape, and complexity in composition are needed to further explore the potential of these materials.

homogeneous heating of the nanostructure is the only way by which plasmonic nanoparticles can affect other non-plasmonic entities in the system (for example, induce chemical reactions on the surface of the nanoparticle)[50,51]. The issue with these arguments is that it has been shown in direct photodiode measurements that hot carriers generated in hybrid plasmonic systems can cross metal/semiconductor Schottky junctions with relatively large barrier heights with non-negligible quantum efficiencies[41,52]. This indicates that energetic, non-thermal charge carriers readily sample the surface (junction) before equilibrating with the phonon modes. Additionally, substantial increases in the rates of chemical transformations on the surface of plasmonic nanoparticles, changes in product selectivity, and very high kinetic isotope effects in light driven reactions, which cannot be fully explained by a macroscopic heating of phonon modes, have been reported[53–61].

To properly model and explain the behaviour of the multicomponent plasmonic systems, it is necessary to recognize that two (or more) components give rise to spatially non-homogeneous physical properties, which, at the femtosecond-temporal and atomic-spatial

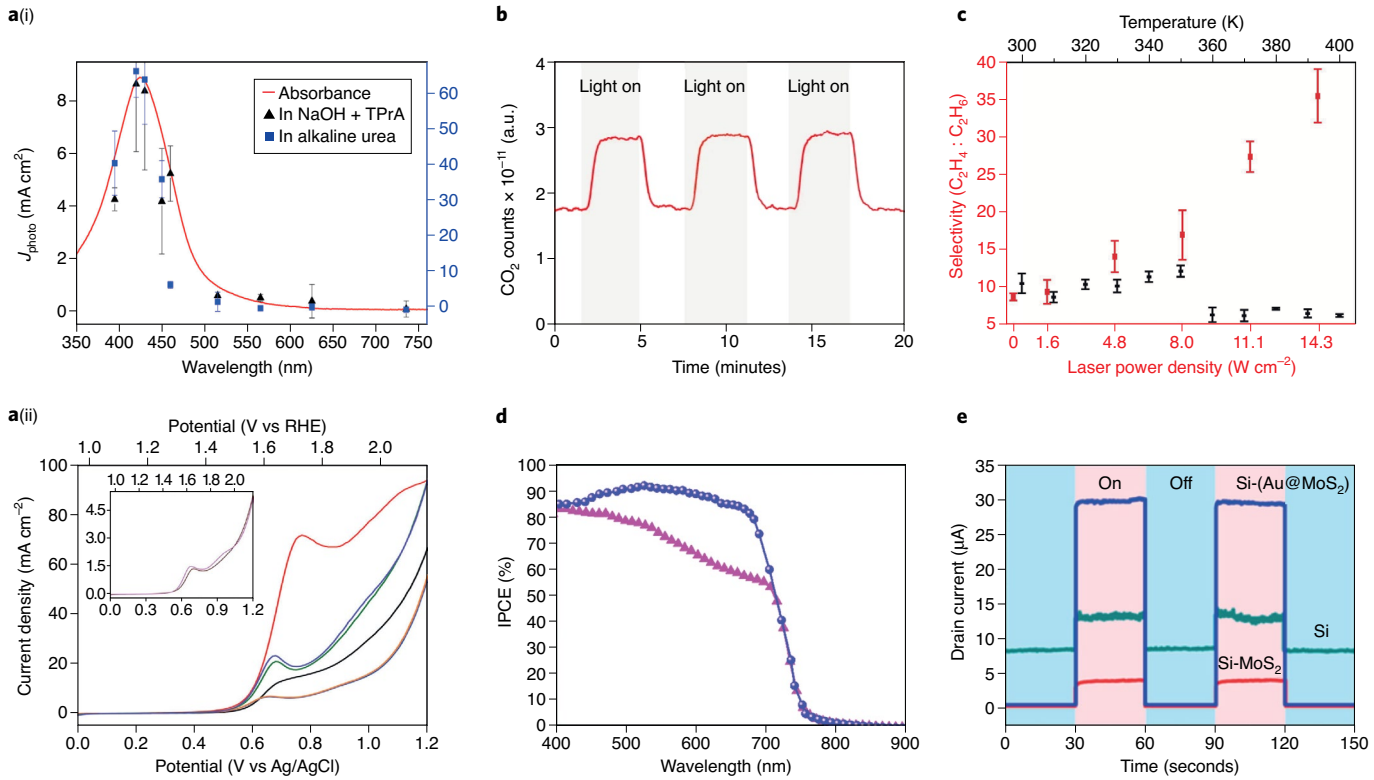

Fig. 5 | Applications of hybrid plasmonic materials. a, Photocatalytic urea oxidation using plasmonic 'nanopigments' consisting of an Ag nanoparticle core surrounded with molecular tris(bipyridine)ruthenium(II) ($[Ru(bpy)_3]^{2+}$) photocatalyst at the surface, embedded in a phospholipid membrane scaffold/spacer layer. (i) Current (reaction rate in urea photo-oxidation) was measured for nanopigments under illumination and compared to lipid-wrapped Ag with no $[Ru(bpy)_3]^{2+}$ (LipoAg), a physical mixture of Ag nanoparticles and $[Ru(bpy)_3]^{2+}$ with no lipid layer (Mixture), and stand-alone $[Ru(bpy)_3]^{2+}$ (enlarged curves in figure inset). (ii) Photocurrent densities (reaction rate, J_{photo}) as a function of wavelength for nanopigments in two different electrolytes, correlated closely with the plasmon absorbance of the nanopigment structure. **b**, Reaction rate (measured in CO_2 production counts) for the preferential oxidation of CO in excess H_2 on Ag–Pt core-shell nanoparticles during the periodic cycling of light-on and light-off conditions. Similar tests on monometallic Ag nanoparticles showed no rate for CO_2 production under identical conditions, indicating the reaction occurred only on the Pt surface of the Ag-Pt nanocubes. **c**, Selectivity to ethylene and ethane products from acetylene hydrogenation under illuminated (red) and thermal (black) conditions on a Pd catalyst coupled to a plasmonic Al antenna (antenna-reactor). **d**, Incident photon-to-electron conversion efficiency (ICPE) of TiO_2 nanorod-functionalized perovskite solar cells with and without additional Au nanoparticles. **e**, The measured current of Si–MoS_2 photodiodes with and without the incorporation of Au nanoparticles under periodic illumination. The Si photodiode without MoS_2 is included as another control. Figure adapted with permission from ref. [73], Cell Press (**a**); ref. [12], Springer Nature Ltd (**b**); ref. [74], PNAS (**c**); ref. [77], RSC (**d**); and ref. [78], American Chemical Society (**e**).

resolutions, impact the initial location of energetic charge carrier formation as well as the flow of these carriers in the system. Assumptions of spatially homogeneous behaviour of these systems (as are often made in the modelling of plasmon heating) or temporal steady-state behaviour, as described above in the context equilibration with the phonon modes before charge is extracted, overlook critical phenomena. A proper model that can capture the behaviour of hybrid plasmonic materials requires adequate representation of both, the plasmonic and non-plasmonic components as well as the interface between them.

Specifically, in modelling the behaviour of these hybrid materials, it is critical to fully describe: (1) the Kreibig decay channel that pushes the plasmon decay (initial hot e–h formation) to the surface of nanoparticles; (2) the importance of the electronic states that allow for the direct fast decay channels (akin to the *d*-to-*s* transitions above) in almost all plasmonic/non-plasmonic hybrid materials and interfaces, which leads to spatially non-homogenous dielectric function; and (3) the non-homogeneous nature of the electric field that drives the optical excitations. The physical situation becomes even more complex when two plasmonic particles are close to each other (~1 nm apart). In these systems, the above-described optically excited metallic polarization, which characterizes one-particle LSPR states, becomes a junction surface polarization, leading to high local fields at the particle junction (that is, the light energy becomes highly concentrated at the junction between the particles)[6]. This concentration of optical energy ('hot spots') can further shift the process of initial e–h formation to these junctions[62].

The extent to which energetic charge carriers sample the plasmonic/non-plasmonic interface is further augmented by the fact that even the energetic charge carriers initially formed in the bulk of the plasmonic component, due to large mean free paths of *s* electrons and holes in plasmonic materials (for example, 50 nm for *s*-orbital electrons in Ag), can reach the surface (interface) without losing energy[31,62,63]. This means that a large fraction of energetic electrons or holes are either initially formed in the non-plasmonic component (or at the interface) or readily sample the interface before losing energy. This can have dramatic consequences. For example, scattering of hot charge carriers through the molecule that resides on the surface of plasmonic metal or the initial formation of these charge hot carriers directly in the molecule can lead to rapid chemical transformations of the molecule[64–67]. These chemical transformations can take place either on charged (or excited) potential energy surfaces or via vibronic coupling within the molecule, wherein a hot electron (or hole) that scatters through the molecule can lead to elevated

molecular heating even without macroscopic heating of the nanostructure[25,30,54,56,68]. There are many contributions supporting this local charge excitation-mediated chemical reaction mechanism[30,69]. In a recent study, Kazuma et al. used scanning tunnelling microscopy (STM) to study the plasmon-induced dissociation of dimethyl disulfide on Ag and Cu surfaces at a phonon system temperature of 5 K (Fig. 3c(i))[69]. The yield of the plasmon enhanced reaction, γ_{LSP}, was observed to be two orders of magnitude higher than the yield of the purely photoinduced process, γ_{photon} (without LSPR—Fig. 3c(ii),(iii)). The wavelength-dependent plasmon-induced yield mapped directly with the in-gap electric field intensity, supporting the role of direct intermolecular excitations at the metal–adsorbate interface in improving efficiencies (Fig. 3c(iv)). Comparable findings have also been reported for the plasmon-induced dissociation of O_2 on Ag with quantum yields reaching up to 1.2%[57]. Similar arguments associated with high probabilities for the initial formation of energetic charge carriers at semiconductor/metal interfaces, discussed above (Fig. 2b,c), can explain the experimentally measured flow of energetic charge carriers across Schottky barriers in metal/semiconductor systems.

In addition to describing the initial location of generated e–h pairs, their energy distribution, and their flow through the nanomaterial, it is also critical to accurately describe how these energetic charge carriers couple to phonon modes. In this context, the field has relied on so-called two temperature models that assume: (1) an electronic energy thermalization, where the exited electronic structure is described in terms of an elevated temperature Fermi–Dirac distribution; and (2) the transfer of this electron energy to a phonon distribution that is described by the equilibrium phonon temperature[70]. While these approximations might be adequate to describe an electron and phonon temperature in monometallic nanoparticles, they are not sufficient to capture the physical or chemical behaviour of hybrid materials as they naturally lead to the above described misconceptions[71,72]. An obvious example of the fallacy of the two-temperature model is the fact that SERS measurements have demonstrated that in many cases, molecules chemically attached to plasmonic nanoparticles are not in thermal equilibrium with the phonon modes of the nanoparticle itself. This suggests a preferential coupling of the SERS photons (via energetic electrons or holes) with the vibrational adsorbate modes compared to the nanoparticle phonon modes. To move the field forward, we need to adequately describe how local electronic excitations couple to local phonon modes.

We showed above that hybrid plasmonic nanostructures can be engineered to 'push' the location of the initial energetic charge carrier formation to the surface or to the non-plasmonic component. In principle, this can be done by any combination of the following three concepts: (1) employing very small nanostructures where Kreibig surface decay is the dominant LSPR decay pathway; (2) creating plasmonic geometries that support very high local plasmon *E* fields at their surface; or (3) embedding another non-plasmonic material with a high imaginary part of the dielectric function, at the surface of plasmonic nanoparticles (Fig. 4a,b). Taking advantage of these opportunities opens avenues for a new generation of hot carrier and energy conversion devices for photocatalysis, photodetectors and photovoltaics. For example, attaching a thin layer of a semiconductor on a plasmonic material should lead to substantial enhancements in the absorption in the semiconductor component of the hybrid nanostructure (Fig. 4b). The question is whether the energetic charge carriers formed in the semiconductor can be extracted (for example, drive redox) reactions before they thermalize to the semiconductor band edge or before they recombine—that is, is it possible to have power efficiencies above the Schockley–Queisser limit?

To begin addressing these questions and to take advantage of these opportunities, multicomponent plasmonic nanostructures need to be designed and synthesized with precise geometries, including shape and size of the plasmonic and non-plasmonic components and an atomistic control over their coupling (Fig. 4c). To accomplish this, major advances in the controlled and scalable synthesis of multicomponent nanostructures need to take place. It is fair to say that the past 30 years of research in the materials science community have been characterized by an extensive focus on synthesis and characterization of single-component nanomaterials. Our ability to fully control the synthesis of multicomponent nanostructures is rather limited to highly expensive and difficult to scale nanofabrication approaches.

Applications of hybrid plasmonic materials

Even with these obstacles, it is encouraging to see multiple recent examples of hybrid plasmonic demonstrations of novel physical and chemical properties. In one of these studies, a classical tris(bipyridine)ruthenium(II) ($[Ru(bpy)_3]^{2+}$) molecular photocatalyst at the surface of Ag nanoparticles, showed a 50-fold enhancement in photon-to-current efficiency compared to standalone $[Ru(bpy)_3]^{2+}$ in photocatalytic oxidation of urea (Fig. 5a)[73]. Similarly, our group has demonstrated that it is possible to drive light-induced chemical transformations on non-plasmonic and non-photo-active Pt surfaces when thin layers of Pt (~1 nm thick) are coated onto Ag nanoparticles (Fig. 5b)[12]. There are similar examples of antenna–reactor photocatalysts, where plasmonic aluminium (Al) nanodiscs (the antenna) are coupled to Pd materials (the reactor) to drive photochemistry on non-photoactive Pd nanoparticles with high selectivity (Fig. 5c)[74,75]. Hybrid plasmonic systems have also been shown to improve the efficiencies of photovoltaics for solar energy conversion and photodetectors for sensing applications[14,34,76–79]. For example, Mali et al. reported the fabrication of perovskite solar cells functionalized with Au-decorated TiO_2 nanorods with internal quantum efficiencies as high as 93% and a corresponding thermodynamic power conversion efficiency of 14% (Fig. 5d)[77]. These efficiencies were ~30% lower for identical samples without plasmonic Au. Furthermore, Li et al. demonstrated that a ten-fold increase in the photocurrent generation (drain current) of a Si–MoS_2 gateless photodiode upon the incorporation of Au nanoparticles[78]. When illuminated with an incident power of 50 μW, the diode photocurrent was measured to be ~3 μA and ~29 μA for the Si–MoS_2 and Si–Au–MoS_2 systems respectively (Fig. 5e). This corresponded to a photoresponsivity of 11.2 A W^{-1} for the Si–Au–MoS_2, two orders of magnitude higher than the previously reported value for monolayer MoS_2 photodetectors[80].

Mechanistic analysis showed that in all these hybrid systems, the transfer of energy between illuminated plasmonic and non-plasmonic components was responsible for the observed plasmon-mediated efficiency enhancements.

In conclusion, current experimental evidence suggests that it is possible to extract energy out of plasmonic nanostructures, characterized by large optical extinction cross-sections, before the energy is thermalized with nanostructure phonon modes. The main reason for this is that the initial formation of energetic e–h pairs within the plasmonic nanostructures seems to be concentrated to a particular location in the system, such as the plasmonic/non-plasmonic interface[12,35,37–39]. To move the field forward, we need to understand how the plasmon energy is distributed in time and space in these systems. It is critical to rigorously assess the geometric locations on the initial formation of energetic charge carriers. As we pointed out in the text above, this requires us to fully appreciate the non-homogeneous nature of the electronic structure (dielectric function) and the optical response (electric field) of plasmonic materials to incident illumination. Furthermore, we need to unearth the fundamental physical factors that govern the propagation of the energy stored in these e–h pairs through multicomponent systems. These fundamental insights will ultimately inform us about the upper limits of energetic charge carrier extraction from hybrid plasmonic systems.

Received: 28 April 2020; Accepted: 16 October 2020;
Published online: 4 January 2021

References

1. Giannini, V., Fernández-Domínguez, A. I., Heck, S. C. & Maier, S. A. Plasmonic nanoantennas: fundamentals and their use in controlling the radiative properties of nanoemitters. *Chem. Rev.* **111**, 3888–3912 (2011).
2. Schuller, J. A. et al. Plasmonics for extreme light concentration and manipulation. *Nat. Mater.* **9**, 193–204 (2010).
3. Linic, S., Christopher, P. & Ingram, D. B. Plasmonic-metal nanostructures for efficient conversion of solar to chemical energy. *Nat. Mater.* **10**, 911–921 (2011).
4. Linic, S., Aslam, U., Boerigter, C. & Morabito, M. Photochemical transformations on plasmonic metal nanoparticles. *Nat. Mater.* **14**, 567–576 (2015).
5. Stiles, P. L., Dieringer, J. A., Shah, N. C. & Van Duyne, R. P. Surface-enhanced Raman spectroscopy. *Annu. Rev. Anal. Chem.* **1**, 601–626 (2008).
6. Brus, L. Noble metal nanocrystals: plasmon electron transfer photochemistry and single-molecule Raman spectroscopy. *Acc. Chem. Res.* **41**, 1742–1749 (2008).
7. Rao, V. G., Aslam, U. & Linic, S. Chemical requirement for extracting energetic charge carriers from plasmonic metal nanoparticles to perform electron-transfer reactions. *J. Am. Chem. Soc.* **141**, 643–647 (2019).
8. Butet, J., Brevet, P.-F. & Martin, O. J. F. Optical second harmonic generation in plasmonic nanostructures: from fundamental principles to advanced applications. *ACS Nano* **9**, 10545–10562 (2015).
9. Celebrano, M. et al. Mode matching in multiresonant plasmonic nanoantennas for enhanced second harmonic generation. *Nat. Nanotechnol.* **10**, 412–417 (2015).
10. Stuart, D. A., Haes, A. J., Yonzon, C. R., Hicks, E. M. & Duyne, R. P. V. Biological applications of localised surface plasmonic phenomenae. *IEE Proc. Nanobiotechnol.* **152**, 13–32 (2005).
11. Kabashin, A. V. et al. Plasmonic nanorod metamaterials for biosensing. *Nat. Mater.* **8**, 867–871 (2009).
12. Aslam, U., Chavez, S. & Linic, S. Controlling energy flow in multimetallic nanostructures for plasmonic catalysis. *Nat. Nanotechnol.* **12**, 1000–1005 (2017).
13. Ndukaife, J. C., Shalaev, V. M. & Boltasseva, A. Plasmonics—turning loss into gain. *Science* **351**, 334–335 (2016).
14. Brongersma, M. L., Halas, N. J. & Nordlander, P. Plasmon-induced hot carrier science and technology. *Nat. Nanotechnol.* **10**, 25–34 (2015).
15. Moskovits, M. The case for plasmon-derived hot carrier devices. *Nat. Nanotechnol.* **10**, 6–8 (2015).
16. Clavero, C. Plasmon-induced hot-electron generation at nanoparticle/metal-oxide interfaces for photovoltaic and photocatalytic devices. *Nat. Photon.* **8**, 95–103 (2014).
17. Nozieres, P. *Theory of Quantum Liquids* (CRC Press, 2018).
18. Kubo, A. et al. Femtosecond imaging of surface plasmon dynamics in a nanostructured silver film. *Nano Lett.* **5**, 1123–1127 (2005).
19. Yannouleas, C. & Broglia, R. A. Landau damping and wall dissipation in large metal clusters. *Ann. Phys.* **217**, 105–141 (1992).
20. Bohren, C. F. How can a particle absorb more than the light incident on it? *Am. J. Phys.* **51**, 323–327 (1983).
21. Jain, P. K., Lee, K. S., El-Sayed, I. H. & El-Sayed, M. A. Calculated absorption and scattering properties of gold nanoparticles of different size, shape, and composition: applications in biological imaging and biomedicine. *J. Phys. Chem. B* **110**, 7238–7248 (2006).
22. Khurgin, J. B. How to deal with the loss in plasmonics and metamaterials. *Nat. Nanotechnol.* **10**, 2–6 (2015).
23. Hartland, G. V. Optical studies of dynamics in noble metal nanostructures. *Chem. Rev.* **111**, 3858–3887 (2011).
24. Abelès, F. *Optical Properties of Solids* (Elsevier, 1972).
25. Boerigter, C., Campana, R., Morabito, M. & Linic, S. Evidence and implications of direct charge excitation as the dominant mechanism in plasmon-mediated photocatalysis. *Nat. Commun.* **7**, 10545 (2016).
26. Kambhampati, P., Child, C. M., Foster, M. C. & Campion, A. On the chemical mechanism of surface enhanced Raman scattering: experiment and theory. *J. Chem. Phys.* **108**, 5013–5026 (1998).
27. Khurgin, J. B. & Levy, U. Generating hot carriers in plasmonic nanoparticles: when quantization does matter? *ACS Photon.* **7**, 547–553 (2020).
28. Trolle, M. L. & Pedersen, T. G. Indirect optical absorption in silicon via thin-film surface plasmon. *J. Appl. Phys.* **112**, 043103 (2012).
29. Khurgin, J. B. & Sun, G. Scaling of losses with size and wavelength in nanoplasmonics and metamaterials. *Appl. Phys. Lett.* **99**, 211106 (2011).
30. Boerigter, C., Aslam, U. & Linic, S. Mechanism of charge transfer from plasmonic nanostructures to chemically attached materials. *ACS Nano* **10**, 6108–6115 (2016).
31. Brown, A. M., Sundararaman, R., Narang, P., Goddard, W. A. & Atwater, H. A. Nonradiative plasmon decay and hot carrier dynamics: effects of phonons, surfaces, and geometry. *ACS Nano* **10**, 957–966 (2016).
32. Foerster, B., Spata, V. A., Carter, E. A., Sönnichsen, C. & Link, S. Plasmon damping depends on the chemical nature of the nanoparticle interface. *Sci. Adv.* **5**, eaav0704 (2019).
33. Sundararaman, R., Narang, P., Jermyn, A. S., Goddard, W. A. III & Atwater, H. A. Theoretical predictions for hot-carrier generation from surface plasmon decay. *Nat. Commun.* **5**, 5788 (2014).
34. Narang, P., Sundararaman, R. & Atwater, H. A. Plasmonic hot carrier dynamics in solid-state and chemical systems for energy conversion. *Nanophotonics* **5**, 96–111 (2016).
35. Chavez, S., Aslam, U. & Linic, S. Design principles for directing energy and energetic charge flow in multicomponent plasmonic nanostructures. *ACS Energy Lett.* **3**, 1590–1596 (2018).
36. Christopher, P. & Moskovits, M. Hot charge carrier transmission from plasmonic nanostructures. *Annu. Rev. Phys. Chem.* **68**, 379–398 (2017).
37. Chavez, S., Govind Rao, V. & Linic, S. Unearthing the factors governing site specific rates of electronic excitations in multicomponent plasmonic systems and catalysts. *Faraday Discuss.* **214**, 441–453 (2019).
38. Tan, S. et al. Plasmonic coupling at a metal/semiconductor interface. *Nat. Photon.* **11**, 806–812 (2017).
39. Foerster, B. et al. Interfacial states cause equal decay of plasmons and hot electrons at gold–metal oxide interfaces. *Nano Lett.* **20**, 3338–3343 (2020).
40. Engelbrekt, C., Crampton, K. T., Fishman, D. A., Law, M. & Apkarian, V. A. Efficient plasmon-mediated energy funneling to the surface of Au@Pt core–shell nanocrystals. *ACS Nano* **14**, 5061–5074 (2020).
41. Wu, K., Chen, J., McBride, J. R. & Lian, T. Efficient hot-electron transfer by a plasmon-induced interfacial charge-transfer transition. *Science* **349**, 632–635 (2015).
42. Foerster, B. et al. Chemical interface damping depends on electrons reaching the surface. *ACS Nano* **11**, 2886–2893 (2017).
43. Hendrich, C. et al. Chemical interface damping of surface plasmon excitation in metal nanoparticles: a study by persistent spectral hole burning. *Appl. Phys. B* **76**, 869–875 (2003).
44. Stietz, F. et al. Decay times of surface plasmon excitation in metal nanoparticles by persistent spectral hole burning. *Phys. Rev. Lett.* **84**, 5644–5647 (2000).
45. Ziegler, T., Hendrich, C., Hubenthal, F., Vartanyan, T. & Träger, F. Dephasing times of surface plasmon excitation in Au nanoparticles determined by persistent spectral hole burning. *Chem. Phys. Lett.* **386**, 319–324 (2004).
46. Therrien, A. J. et al. Impact of chemical interface damping on surface plasmon dephasing. *Faraday Discuss.* **214**, 59–72 (2019).
47. Moskovits, M. & DiLella, D. P. in *Surface Enhanced Raman Scattering* (eds Chang, R. K. & Furtak, T. E.) 243–273 (Springer, 1982).
48. Xu, H., Aizpurua, J., Käll, M. & Apell, P. Electromagnetic contributions to single-molecule sensitivity in surface-enhanced Raman scattering. *Phys. Rev. E* **62**, 4318–4324 (2000).
49. Nie, S. & Emory, S. R. Probing single molecules and single nanoparticles by surface-enhanced Raman scattering. *Science* **275**, 1102–1106 (1997).
50. Sivan, Y., Un, I. W. & Dubi, Y. Assistance of metal nanoparticles in photocatalysis – nothing more than a classical heat source. *Faraday Discuss.* **214**, 215–233 (2019).
51. Dubi, Y. & Sivan, Y. "Hot" electrons in metallic nanostructures—non-thermal carriers or heating? *Light Sci. Appl.* **8**, 89 (2019).
52. Tagliabue, G. et al. Quantifying the role of surface plasmon excitation and hot carrier transport in plasmonic devices. *Nat. Commun.* **9**, 3394 (2018).
53. Cortes et al. Plasmonic hot electron transport drives nano-localized chemistry. *Nat. Commun.* **8**, 14880 (2017).
54. Christopher, P., Xin, H. & Linic, S. Visible-light-enhanced catalytic oxidation reactions on plasmonic silver nanostructures. *Nat. Chem.* **3**, 467–472 (2011).
55. Mukherjee, S. et al. Hot electrons do the impossible: plasmon-induced dissociation of H_2 on Au. *Nano Lett.* **13**, 240–247 (2013).
56. Christopher, P., Xin, H., Marimuthu, A. & Linic, S. Singular characteristics and unique chemical bond activation mechanisms of photocatalytic reactions on plasmonic nanostructures. *Nat. Mater.* **11**, 1044–1050 (2012).
57. Seemala, B. et al. Plasmon-mediated catalytic O_2 dissociation on Ag nanostructures: hot electrons or near fields? *ACS Energy Lett.* **4**, 1803–1809 (2019).
58. Zhou, L. et al. Quantifying hot carrier and thermal contributions in plasmonic photocatalysis. *Science* **362**, 69–72 (2018).
59. Kim, Y., Smith, J. G. & Jain, P. K. Harvesting multiple electron–hole pairs generated through plasmonic excitation of Au nanoparticles. *Nat. Chem.* **10**, 763–769 (2018).
60. Marimuthu, A., Zhang, J. & Linic, S. Tuning selectivity in propylene epoxidation by plasmon mediated photo-switching of Cu oxidation state. *Science* **339**, 1590–1593 (2013).
61. Kale, M. J., Avanesian, T. & Christopher, P. Direct photocatalysis by plasmonic nanostructures. *ACS Catal.* **4**, 116–128 (2014).
62. Hartland, G. V., Besteiro, L. V., Johns, P. & Govorov, A. O. What's so hot about electrons in metal nanoparticles? *ACS Energy Lett.* **2**, 1641–1653 (2017).

63. Jermyn, A. S. et al. Transport of hot carriers in plasmonic nanostructures. *Phys. Rev. Mater.* **3**, 075201 (2019).
64. Bonn, M. et al. Phonon- versus electron-mediated desorption and oxidation of CO on Ru(0001). *Science* **285**, 1042–1045 (1999).
65. Hatch, S. R., Zhu, X. Y., White, J. M. & Campion, A. Photoinduced pathways to dissociation and desorption of dioxygen on silver (110) and platinum (111). *J. Phys. Chem.* **95**, 1759–1768 (1991).
66. Zhou, X.-L., Zhu, X.-Y. & White, J. M. Photochemistry at adsorbate/metal interfaces. *Surface Sci. Rep.* **13**, 73–220 (1991).
67. Denzler, D. N., Frischkorn, C., Hess, C., Wolf, M. & Ertl, G. Electronic excitation and dynamic promotion of a surface reaction. *Phys. Rev. Lett.* **91**, 226102 (2003).
68. Aslam, U., Rao, V. G., Chavez, S. & Linic, S. Catalytic conversion of solar to chemical energy on plasmonic metal nanostructures. *Nat. Catal.* **1**, 656–665 (2018).
69. Kazuma, E., Jung, J., Ueba, H., Trenary, M. & Kim, Y. Real-space and real-time observation of a plasmon-induced chemical reaction of a single molecule. *Science* **360**, 521–526 (2018).
70. Anisimov, S. I. & Rethfeld, B. Theory of ultrashort laser pulse interaction with a metal. In *Nonresonant Laser-Matter Interaction (NLMI-9)* Vol. 3093 (ed. Libenson, M. N.) 192–203 (International Society for Optics and Photonics, 1997).
71. Brown, A. M. et al. Experimental and ab initio ultrafast carrier dynamics in plasmonic nanoparticles. *Phys. Rev. Lett.* **118**, 087401 (2017).
72. Frischkorn, C. & Wolf, M. Femtochemistry at metal surfaces: nonadiabatic reaction dynamics. *Chem. Rev.* **106**, 4207–4233 (2006).
73. An, X., Stelter, D., Keyes, T. & Reinhard, B. M. Plasmonic photocatalysis of urea oxidation and visible-light fuel cells. *Chem* **5**, 2228–2242 (2019).
74. Swearer, D. F. et al. Heterometallic antenna–reactor complexes for photocatalysis. *Proc. Natl Acad. Sci. USA* **113**, 8916–8920 (2016).
75. Sytwu, K., Vadai, M. & Dionne, J. A. Bimetallic nanostructures: combining plasmonic and catalytic metals for photocatalysis. *Adv. Phys. X* **4**, 1619480 (2019).
76. Li, W. & Valentine, J. G. Harvesting the loss: surface plasmon-based hot electron photodetection. *Nanophotonics* **6**, 177–191 (2017).
77. Mali, S. S., Shim, C. S., Kim, H., Patil, P. S. & Hong, C. K. *In situ* processed gold nanoparticle-embedded TiO_2 nanofibers enabling plasmonic perovskite solar cells to exceed 14% conversion efficiency. *Nanoscale* **8**, 2664–2677 (2016).
78. Li, Y. et al. Superior plasmonic photodetectors based on Au@MoS_2 core–shell heterostructures. *ACS Nano* **11**, 10321–10329 (2017).
79. Atwater, H. A. & Polman, A. Plasmonics for improved photovoltaic devices. *Nat. Mater.* **9**, 205–213 (2010).
80. Lopez-Sanchez, O., Lembke, D., Kayci, M., Radenovic, A. & Kis, A. Ultrasensitive photodetectors based on monolayer MoS_2. *Nat. Nanotechnol.* **8**, 497–501 (2013).

Acknowledgements

The work presented in this document was supported by the National Science Foundation (NSF) (CHE-1800197). Secondary support was provided by the US Department of Energy, Office of Science, Office of Basic Energy Sciences (DE-SC0021362) (analysis of optical interactions of materials with light) and the Office of Basic Energy Science, Division of Chemical Sciences (DE-SC0021008) (materials synthesis).

Author contributions

S.L. wrote the manuscript. All authors were involved in discussions, gathering of literature and figure design.

Competing interests

The authors declare no competing interests.

Additional information

Correspondence should be addressed to S.L.

Peer review information *Nature Materials* thanks Emiliano Cortés, Prineha Narang and Sebastian Schlücker for their contribution to the peer review of this work.

Reprints and permissions information is available at www.nature.com/reprints.

Publisher's note Springer Nature remains neutral with regard to jurisdictional claims in published maps and institutional affiliations.